JOURNAL OF MATERIALS SCIENCE 30 (1995) 701–711

Rheology of polypropylene in the solid state

P. DUFFO, B. MONASSE, J. M. HAUDIN
Ecole des Mines de Paris, Centre de Mise en Forme des Matériaux (URA CNRS 1374), BP 207, 06904 SOPHIA ANTIPOLIS, France

C. G'SELL, A. DAHOUN
Ecole des Mines de Nancy, Laboratoire de Métallurgie Physique & Science des Matériaux (URA CNRS 155), Parc de Saurupt, 54042 NANCY, France

The tensile behaviour of a commercial grade of isotactic polypropylene was tested in a temperature range between 20 and 150 °C with a video-controlled testing system which is capable of imposing a constant true strain-rate within the neck automatically. The results are displayed in the form of effective stress–strain curves and modelled by a constitutive equation in a multiplicative form. It is thus shown that, for each temperature, the plastic response can be described up to very large strains ($\varepsilon \simeq 2.0$) by a set of four parameters. The assumptions introduced in this modelling are critically discussed in order to check the validity of the simplifying hypotheses (strain homogeneity, isochoric deformation, etc.). The constitutive equation thus obtained was utilized in a finite difference code in order to predict the development of stretching instabilities of polypropylene. The simulation gives access to the engineering stress–strain response of the stretched test piece and to the detailed kinetics of the incipient neck. It is found that the severity of the instabilities is less at room temperature than near the melting point because of the decrease of the strain-hardening and of the strain-rate sensitivity with temperature.

1. Introduction

Tensile testing has been widely used to characterize the mechanical properties of solid polymers. Generally the load–elongation data are only transformed into engineering (or "nominal") stress–strain curves by dividing the load and the elongation by the initial cross-section and initial length, respectively. These engineering curves are interesting from a practical point of view but, due to the early occurrence of necking, they do not provide a correct description of the mechanical behaviour of the material which requires the measurement of the "true stress" and "true strain" in local terms [1].

In view of assessing the intrinsic response of polymers, an early method was proposed by Meinel and Peterlin [2], who determined the "true" flow curve of high-density polyethylene by means of a photographic technique. Their method involved the measurement of the current distances between ink dots printed on the specimen prior to deformation. This approach was criticized by G'Sell and Jonas [3], essentially because the tests had been performed at constant cross-head velocity, so that the local strain rate appeared to vary by one or two orders of magnitude, and the tensile stress had therefore to be tediously corrected for this rate variation in view of obtaining the intrinsic behaviour of the material for a prescribed strain rate. Subsequently, G'Sell and Jonas proposed a new tensile method [3] in which a constant true strain rate was precisely regulated locally in the centre of the tensile specimen. The major interest of the tests at constant local strain rate is to allow the derivation of constitutive equations for the polymer in the solid state [1, 3–5]. Such equations are more particularly required for the modelling of different problems of plastic deformation. Among them, the initiation and propagation of necking are of prime importance from both theoretical and practical points of view (for instance, for the stretching of fibres and films). Different approaches have been proposed: analytical derivations [6–9], finite-difference scheme [5], finite-element method [10–15]. Another domain of application concerns compression, especially for forging simulations [12, 13, 16–18], and more recently multiaxial impact [19].

Although the use of rheological coefficients measured in tension can lead to some problems in the modelling of other types of loading, e.g. compression [12, 13], the tensile test constitutes the reference test for the characterization of solid-state rheology. However, for polymers, only a few data are available in the literature, among them the stress–strain curves obtained by Aly-Helal [5] for high-density polyethylene at three temperatures.

The purpose of the present work was to characterize the solid-state rheology of a widely used semi-crystalline polymer, namely polypropylene, as a function of temperature. Experimental stress–strain curves, recorded in uniaxial tension at different strain rates by means of a video-controlled testing system, will be presented and modelled through a simple constitutive relation. As an example of the application of such

a relation, the development of stretching instabilities will be subsequently predicted for this polypropylene as a function of temperature.

2. Experimental procedure

2.1. Specimen preparation and characterization

The polypropylene used in the present work is produced by Hoechst under the commercial reference Hostalen PPH 1050. Its melt index, measured at 230 °C under a 2.16 kg load (ASTM-D 1238), is 0.3 g/10 min. It was processed in the shape of cylindrical extruded rods, 20 mm diameter, and exempt of bubbles. Microscopic examination of 8 μm thick microtomed films between crossed polarizers reveals a fine spherulitic structure (Fig. 1), the diameter of the spherulites being equal to about 120 μm. The material was also characterized by wide-angle X-ray scattering with a monochromatic source at $\lambda = 0.179$ nm (Fig. 2a). The diffraction spectrum exhibits the main peaks of the monoclinic α-structure of the isotactic PP (1 1 0, 0 4 0, 1 3 0, 1 1 1, $\bar{1}$ 3 1 + 0 4 1) and no significant trace of the hexagonal β-structure. Superimposed on the crystalline peaks, a large hump is visible which corresponds to the X-rays diffused by the amorphous fraction. Also DSC thermograms were obtained (Fig. 2b) in order to measure the heat of fusion of the polymer: $\Delta H_f = 76.4\ J\ g^{-1}$. With reference to the heat of fusion for fully crystallized polypropylene, $\Delta H_{f_c} = 165\ J\ g^{-1}$ [20], this value corresponds to a degree of crystallinity of 46 wt %. Axisymmetrical hourglass-shaped tensile specimens were machined out of extruded rods, with a minimum diameter $D_0 = 6$ mm and an initial radius of curvature $R_{c_0} = 20$ mm (Fig. 3). As a result of this particular shape, the neck was always initiated at the middle of the gauge length, where the cross-section is minimum.

2.2. Determination of the effective strain and stress from the experimental measurements

As stated in a previous work [3] the variations of the effective stress, σ, and strain, ε, at the minimum section of an hourglass-shaped specimen can be readily

Figure 1 Spherulite morphology in the extruded polypropylene.

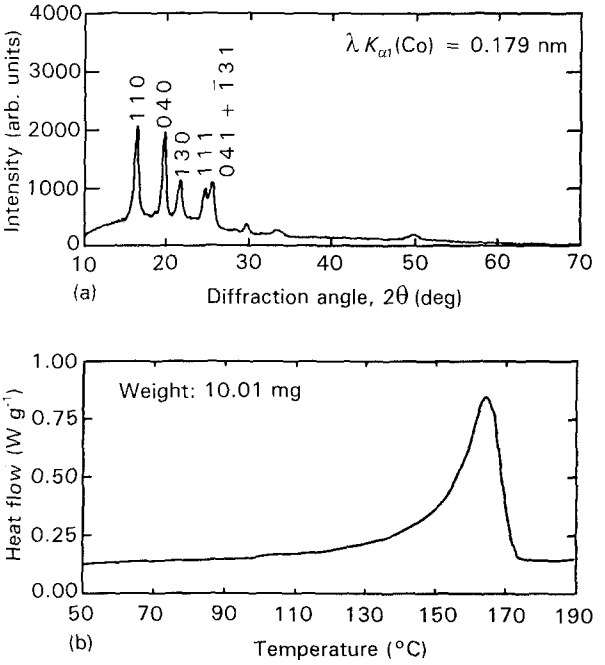

Figure 2 (a) Wide-angle X-ray scattering spectrum of the material. (b) DSC melting curve obtained at a scanning rate of 10 °C min^{-1}.

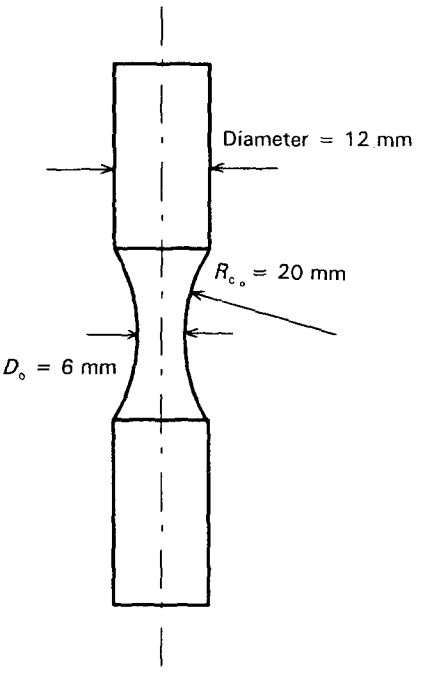

Figure 3 Hourglass-shaped tensile specimen.

derived at any time, t, during a tensile test from the measurements of the minimum diameter $D(t)$, the radius of curvature $R_c(t)$ and the load $F(t)$, providing several reasonable approximations are verified.

Basically, in a sample subjected to homogeneous uniaxial tension, the component of the strain-rate tensor along the axial direction z is expressed through the relative rate of elongation of a given slice of material in the calibrated portion by the relation

$$\dot{\varepsilon}_{zz} = \frac{1}{L}\frac{dL}{dt} \tag{1}$$

where L is the current length of the slice and L_0 its original value. The current deformation, ε_{zz}, is thus

obtained by integration as

$$\varepsilon_{zz} = \int_0^t \dot{\varepsilon}_{zz}(u)\,du = \ln\left(\frac{L}{L_0}\right) \quad (2)$$

Equation 2 is the classical expression of the "true" strain for a standard sample of uniform cross-section over a length L_0, but here we will apply it locally for a thin slice of material situated right at the median plane of the specimen, where the cross-section is minimum. If this slice undergoes an isochoric deformation (that is, if the polymer is supposed to be incompressible), the following equation holds

$$LD^2 = L_0 D_0^2 \quad (3)$$

where D_0 and D are the initial and current diameter of the slice, respectively. It follows from Equations 2 and 3 that

$$\varepsilon_{zz} = 2\ln\left(\frac{D_0}{D}\right) \quad (4)$$

which expresses the local relation between the axial strain and the radial strain $\varepsilon_{rr} = \ln(D/D_0) = -\varepsilon_{zz}/2$. Following the definition associated with the von Mises flow theory the effective strain rate, $\dot{\varepsilon}$, and the effective strain, ε, are expressed by the relations

$$\dot{\varepsilon} = \left[\frac{2}{3}(\dot{e}_{ij}.\dot{e}_{ij})\right]^{1/2} \quad (5)$$

$$\varepsilon = \int_0^t \dot{\varepsilon}(u)du \quad (6)$$

where $\dot{e}_{ij}$ denotes the components of the deviatoric strain-rate tensor. In the particular case of a slice situated in the centre of an hourglass-shaped specimen, the shear components vanish for symmetry reasons. The effective strain rate and strain can thus be approximated by the axial components through the relations

$$\dot{\varepsilon} = \frac{d\varepsilon}{dt} = -\frac{2}{D}\frac{dD}{dt} \quad (7)$$

$$\varepsilon = 2\ln\left(\frac{D_0}{D}\right) \quad (8)$$

In the expression of the effective stress in the same material slice, the direct treatment of the tensile load and the local specimen diameter only gives access to the average axial component $\sigma_{zz} = 4F/\pi D^2$ (sometimes called "true" stress or Kirchoff stress). However, this information is not sufficient to describe the state of stress if the material is locally subjected to a triaxial state of stress, as is the case in the centre of a neck. For a material obeying the von Mises associated flow law, this problem was solved by the introduction of the effective stress, which corresponds to the uniaxial stress which would produce the same effective strain rate as the one generated by the complex triaxial stress field

$$\sigma = \left[\frac{3}{2}(s_{ij}.s_{ij})\right]^{1/2} \quad (9)$$

where s_{ij} denotes the components of the deviatoric stress tensor. It is convenient to characterize the overall effect of triaxiality in the central cross-section of a neck by a scalar factor F_T, called triaxiality factor, which expresses the average ratio of the effective stress to the axial stress. Several expressions for such a factor can be found in the literature [21–25]. The most popular is due to Bridgman [22], who showed that the effective stress is constant in the central slice of the neck provided the following assumptions are verified: (i) the neck is symmetrically concave with a large radius of curvature, (ii) the material is isotropic and rigid-plastic and, (iii) the flow stress is insensitive to strain rate. Under those conditions, F_T is a function of geometrical parameters only and expressed through the relation

$$F_T = 1\Big/\left(1 + \frac{4R_c}{D}\right)\ln\left(1 + \frac{D}{4R_c}\right) \quad (10)$$

As we will show in Section 4, the real case of necks in polypropylene deviates somehow from the ideal situation considered in the latter approach. However, to a first approximation, the Bridgman formula will be considered as operationally valid and we will determine the constitutive relations by means of the following expression

$$\sigma = F_T\frac{4F}{\pi D^2} \quad (11)$$

by which the local effective stress is determined in the same slice as the effective strain from the parameters accessible experimentally.

2.3. Tensile testing system

The minimum diameter of the specimen was measured at room temperature before it was attached to the grips of an MTS servo-hydraulic testing machine (Fig. 4). During the tensile experiments the profile of the tensile samples was followed in real-time by

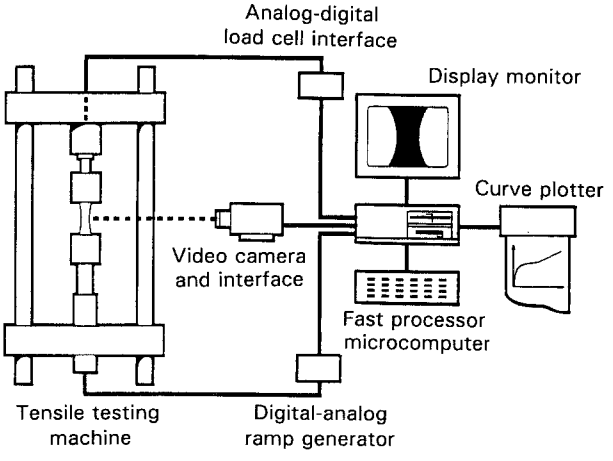

Figure 4 Schematic representation of the video-controlled testing system.

a video camera interfaced with a fast-processor PC computer equipped with an image-digitizing card which makes it possible to determine, at any time t, the profile of the samples and to assess the minimum diameter $D(t)$ and the local radius of curvature $R_c(t)$. From the latter couple of geometric data, the system computed dynamically the variations of the Bridgman triaxiality factor. Moreover, thanks to a ramp generator controlled by an internal clock, the velocity of the hydraulic actuator is automatically adjusted in such a way to keep the strain rate $\dot{\varepsilon}(t)$ constant in the minimum section of the specimen. The computer is also interfaced with the load cell of the MTS machine (maximum load 50 kN). A detailed description of this system has been given elsewhere [26].

The tensile tests were performed at different temperatures in an oven heated by convected hot air. The small volume of this oven allowed minimization of the pre-heating time and optimization of the temperature regulation ($\pm$ 0.5 °C). It was equipped with two windows on the front and rear faces for the videometric inspection of the specimen profile. During the pre-heating of the specimen (for about 20 min), the thermal expansion of the polymer was dynamically compensated by a small displacement of the actuator in order to keep the load equal to zero.

The data displayed on the computer-control monitor were the following: the specimen profile at a given time t, the $\varepsilon(t)$ curve and the $\sigma(\varepsilon)$ curve. In all the tests, the $\varepsilon(t)$ curve was checked to be linear to a very good approximation, which proves that the local strain rate, $\dot{\varepsilon}(t)$, was actually constant. The files containing these curves were eventually transferred from the PC to a VAX computer (Digital Equipment), in order to allow a complete mathematical treatment and particularly to derive the constitutive equation.

3. Results

3.1. Variations of the profile and the triaxiality factor

As an illustration of the capacity of the experimental system, the specimen profiles recorded at different deformation stages are displayed in Fig. 5 for $T = 150\,°C$ and $\dot{\varepsilon} = 5 \times 10^{-4}\,s^{-1}$. The corresponding variations of the Bridgman triaxiality factor are given in Fig. 6 among other curves obtained at different temperatures. Because of the special specimen shape, the Bridgman factor is initially equal to 0.964. It increases in the viscoelastic domain ($\varepsilon \leqslant 0.2$), then decreases due to the occurrence of necking which induces a rapid decrease of the local radius of curvature. It reaches a minimum of about 0.94–0.95 in the strain range between 0.7 and 1.2, and eventually increases again when the shoulders of the neck propagate towards the sample extremities. At the end of the experiment the central part of the specimen exhibits a roughly cylindrical shape and F_T becomes close to unity. From the variations of F_T with temperature, it appears that the location of the minimum shifts towards higher deformations when temperature increases, which means that the neck stabilizes later. A decrease of the minimum value is observed in the temperature range from 20–110 °C, but the values at 110 and 150 °C are similar.

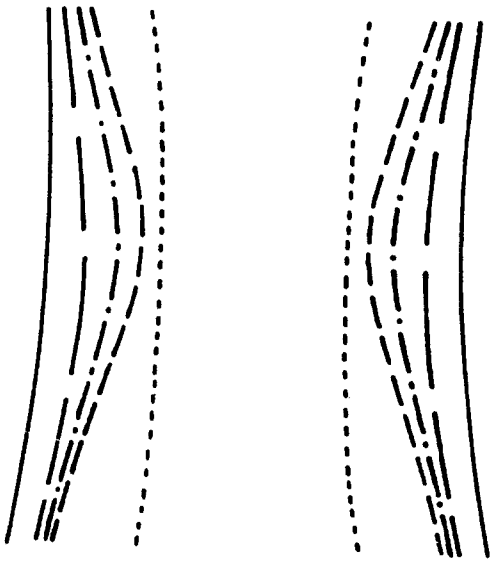

Figure 5 Specimen profiles recorded for different values of ε: (——) 0.00, (— —) 0.39, (— · —) 0.80, (– – –) 1.18, (- - - -) 1.59. ($T = 150\,°C$; $\dot{\varepsilon} = 5 \times 10^{-4}\,s^{-1}$)

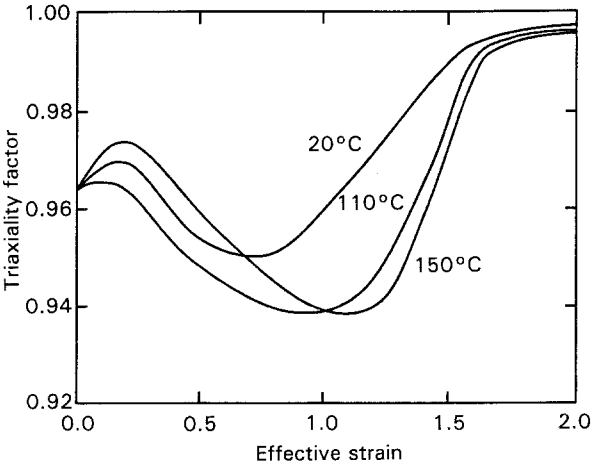

Figure 6 Variations of the Bridgman triaxiality factor with ε for different temperatures ($\dot{\varepsilon} = 5 \times 10^{-4}\,s^{-1}$).

3.2. True stress–strain curves

The tensile behaviour of polypropylene was studied at five temperatures: 20, 80, 110, 130 and 150 °C. For each temperature, different values of $\dot{\varepsilon}$ ranging from 10^{-5}–$10^{-3}\,s^{-1}$ were chosen (Table I). The lower limit

TABLE I Tensile experiments

Temperature	$\dot{\varepsilon}(s^{-1})$					
(°C)	10^{-3}	5×10^{-4}	2×10^{-4}	10^{-4}	5×10^{-5}	10^{-5}
20	×	×		×	×	
80	×	×		×	×	
110	×	×		×	×	
130	×		×	×□		□
150	×	×		□		□

(□) Obtained by strain-rate jumps in the course of a tensile test at a faster strain rate.

was imposed by the total duration of the tensile experiment, which should not exceed 24 h, especially at high temperature because of polymer degradation. To avoid this problem, a technique of strain-rate down-jumps was utilized in several cases during regular speed experiments, for which the $\sigma(\varepsilon)$ curve corresponding to the slow strain-rate was recorded during a limited time only. In the present work, at 130 and 150 °C, the lowest values of $\dot{\varepsilon}$ (10^{-4} s^{-1} and 10^{-5} s^{-1}) were obtained in such jumps from an initial value of 10^{-3} s^{-1}. These experiments are indicated by square symbols in Table I. The upper limit was deduced from the works of Aly-Helal [5] and Marquez-Lucero *et al.* [27] who showed from detailed dynamometric analyses and thermographic measurements that isothermal tests, exempt of significant self-heating, can be performed only if the plastic strain rate is lower than about 5×10^{-3} s^{-1}.

Figs 7 and 8 present typical effective stress–strain curves determined as indicated in the above section.

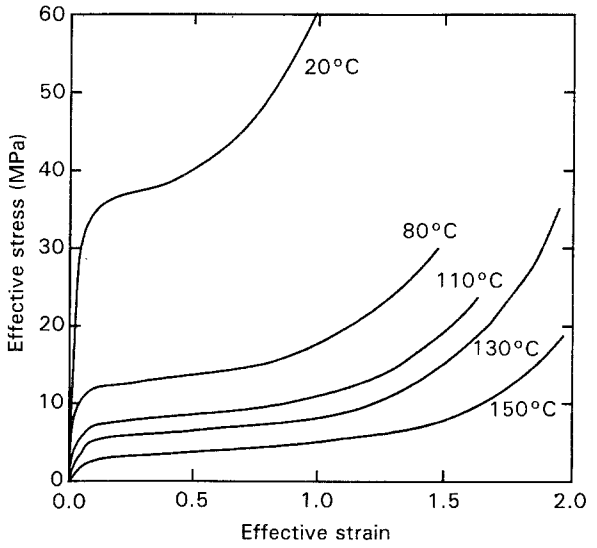

Figure 7 Typical effective stress versus effective strain curves determined at different temperatures for a constant strain rate $\dot{\varepsilon} = 10^{-3}$ s^{-1}.

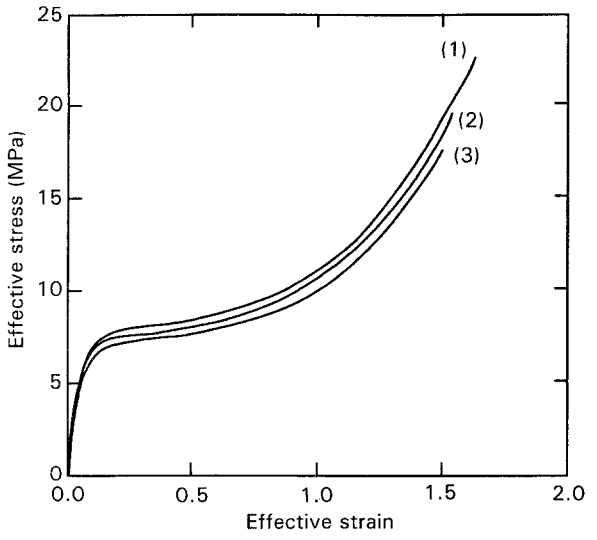

Figure 8 Typical effective stress versus effective strain curves determined at 110 °C for different strain rates: (1) 10^{-3} s^{-1}, (2) 5×10^{-4} s^{-1}, (3) 10^{-4} s^{-1}.

They exhibit the classical shape commonly observed for semi-crystalline polymers [1, 3–5]: the polymer yields progressively with a very gradual transition between the viscoelastic and plastic regions and no stress drop is observed. More specifically, these figures show the respective influences of temperature, T, and strain-rate, $\dot{\varepsilon}$, on the $\sigma(\varepsilon)$ curves

at a given strain rate and a given strain, the stress decreases rapidly when the temperature increases (Fig. 7),

at a given temperature and a given strain, the stress increases moderately with increasing strain-rates (Fig. 8).

3.3. Determination of the constitutive equations

A major interest of the effective stress–strain curves determined at constant strain-rate is the possibility to derive a constitutive equation directly, in the form of a mathematical equation relating σ to ε and $\dot{\varepsilon}$. Two types of analytical laws have been proposed in the literature and applied to solid polymers: the multiplicative type [1, 3, 5, 6, 25, 28, 29] and the additive type [4, 5, 30, 31]. In the first case, the influences of strain and strain rate are separated in a multiplicative way

$$\sigma(\varepsilon, \dot{\varepsilon}) = f(\varepsilon) \times g(\dot{\varepsilon}) \tag{12}$$

whereas for the additive law:

$$\sigma(\varepsilon, \dot{\varepsilon}) = f'(\varepsilon) + g'(\dot{\varepsilon}) \tag{13}$$

In the present work, a multiplicative form was preferred because it is more convenient for computer simulations, as we will discuss later. The following expression of the constitutive equation was chosen [5, 6]

$$\sigma(\varepsilon, \dot{\varepsilon}) = k[1 - \exp(-w\varepsilon)] \exp(h\varepsilon^2)(\dot{\varepsilon}/\dot{\varepsilon}_0)^m \tag{14}$$

where k is a scaling factor, $[1 - \exp(-w\varepsilon)]$ is a "viscoelastic" term which describes the beginning of the σ–ε curve (it is equal to zero for $\varepsilon = 0$ and rapidly tends to 1 when ε increases), $\exp(h\varepsilon^2)$ takes into account the very important strain-hardening observed at large deformations. Finally, the term $(\dot{\varepsilon}/\dot{\varepsilon}_0)^m$ expresses the strain-rate sensitivity as a power law, the reference strain rate, $\dot{\varepsilon}_0$ (conventionally equal to 1 s^{-1}), being introduced for equation homogeneity. Consequently, the constitutive equation at a given temperature depends on four rheological coefficients only: the scaling factor k, the viscoelastic coefficient w, the strain-hardening parameter h and the strain-rate sensitivity coefficient m. These parameters are determined from the experimental $\sigma(\varepsilon)$ curves by the procedure indicated below.

For a given temperature, T, and at a given strain, ε, the variations of $\ln(\sigma)$ are plotted as a function of $\ln(\dot{\varepsilon})$. The curve thus obtained appears to be a straight line whose slope is m. If the multiplicative law (Equation 14) were strictly obeyed, m should be a constant. In fact, it may fluctuate somehow with ε, so that the

average value of m is taken into consideration in the constitutive equation.

At large strains, the viscoelastic term is practically equal to 1 (typically at $\varepsilon \geqslant 0.2$ for $20 \leqslant w \leqslant 50$). In this strain domain, $\ln[\sigma/k(\dot{\varepsilon}/\dot{\varepsilon}_0)^m]$ is plotted against ε^2 for given temperature and strain rate. The curve is fitted by a straight line whose slope and ordinate give h and $\ln(k)$, respectively. Here again, the parameters h and k may show some fluctuations with $\dot{\varepsilon}$ and the average values over the strain-rate range are recorded.

Conversely, at low strains, the viscoelastic term varies between 0 and 1, and the strain-hardening factor is close to 1. In the strain range where $\exp(h\varepsilon^2)$ is lower than 1.01, and for given temperature and strain rate, $\ln\{1 - [\sigma/(\dot{\varepsilon}/\dot{\varepsilon}_0)^m]\}$ is plotted as a function of ε, with k and m being the values determined above. The slope of this straight line $(-w)$ gives access to the viscoelastic term, w, whose operational value is finally obtained by averaging over the $\dot{\varepsilon}$ range.

The procedure presented above was applied to the experimental stress–strain curves obtained with the polypropylene samples for the strain rate and temperature range under investigation. The best fitted values obtained for the parameters are displayed in Table II. It should be noted, however, that their precision is variable. It is fairly good for k and h, the fluctuations of these parameters with $\dot{\varepsilon}$ being less than about 6% and 10%, respectively. Conversely, as stated before by Aly-Helal [5], the viscoelastic coefficient, w, is affected by erratic variations with $\dot{\varepsilon}$ which can be as high as 40%. This is because the determination of w is based on a limited portion of the $\sigma(\varepsilon)$ curves, within a range of small strains where the precision of the videometric method is limited. As for the strain-rate sensitivity coefficient, m, its fluctuations with strain were analysed carefully: at room temperature a gradual increase of m with ε is recorded, the deviation from the average value being smaller than 20%. While approaching the melting point, the fluctuations become more erratic, with a standard deviation which may be as high as 40% in a few cases. In general terms, the evaluation of m is a serious task which requires numerous tests in a range of strain rates as large as possible. Unfortunately, this cannot be achieved readily because the tests at fast strain rates are eventually affected by self-heating effects, while the extremely slow experiments, not only are limited by thermal degradation, but also are sensitive to experimental artefacts (long-term temperature drift, electric power cut, etc). In order to check the correctness of the constitutive equation, the modelled stress–strain curves corresponding to the set of parameters indicated in Table II are displayed in Fig. 9.

TABLE II Rheological coefficients of polypropylene

	T(°C)				
	20	80	110	130	150
k(MPa)	63.6	17.4	9.1	7.5	4.5
h	0.52	0.36	0.39	0.45	0.40
m	0.082	0.047	0.029	0.040	0.034
w	31	32	33	26	23

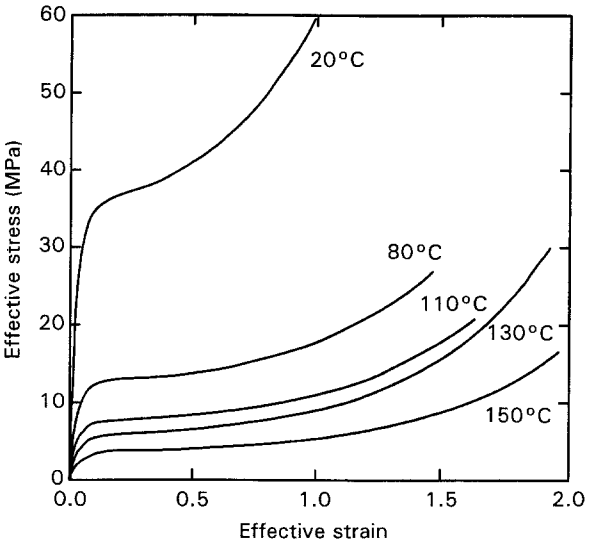

Figure 9 Theoretical stress–strain curves determined from the constitutive Equation 14 for the same conditions as the experimental curves of Fig. 7.

4. Discussion

4.1. Validity of the basic assumptions

It is clear from the preceding section that the determination of the constitutive relations relies on the appropriate definitions of the effective strain and stress. The assumptions on which these definitions are based will be now discussed.

As far as the strain is concerned, the calculation of $\dot{\varepsilon}$ and ε from the experimental data implies two hypotheses: the deformation is locally homogeneous and the material is non-compressible. The problem of the local homogeneity of the deformation can be discussed from two combined viewpoints, microstructural and mechanical. From a microstructural point of view, it is well known that the polymer deformation during uniaxial drawing is intrinsically inhomogeneous at different scales [32]: in the neck, the initial spherulitic morphology is transformed into a microfibrillar structure. Moreover, the deformation within each individual spherulite is not homogeneous and depends on the orientation with respect to the tensile axis. Therefore our approach implies that a thin slice perpendicular to the tensile axis corresponds to a given stage of the spherulitic to microfibrillar transformation and that the "macroscopic" strain, ε, averages the intraspherulitic deformation [1].

To be actually representative of the deformation state, ε should be constant within the slice, i.e. dependent on z only. To check this point a finite element calculation was performed in the case of an elastoplastic behaviour [11]. The local effective strain, $\varepsilon(r)$, was calculated for different sections perpendicular to the tensile axis and compared to the value given by Equation 8. It was found that the computed effective strain is fairly constant over sections corresponding to weak curvatures (e.g. at the inflexion point of the profile) but shows some variation in the centre of the neck.

Similar results were obtained by Laugier [13] using a viscoplastic approach. Such effects have been previously discussed in the literature for the case of metals

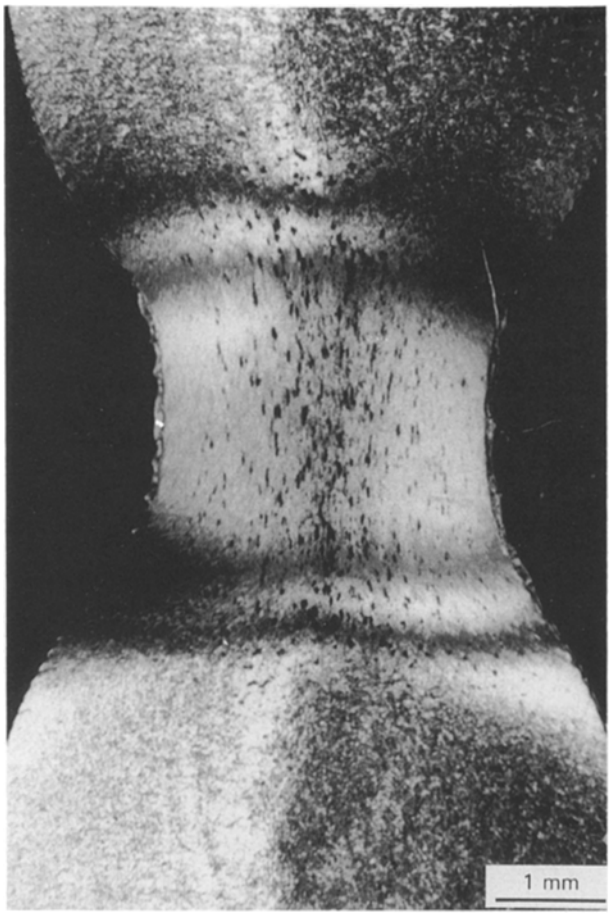

Figure 10 Polarized transmission micrograph of a thin polypropylene film cut along the axis of a necked sample ($T = 20\,°C$; $\varepsilon = 1.37$).

(e.g. [33]). They are associated with the different strain paths followed by material elements located at different initial radial and axial coordinates. Experimentally, in the present case of polypropylene, an interesting micrograph is presented in Fig. 10 in the particular case of a sample subjected to tension at 20 °C up to a local strain $\varepsilon = 1.37$. This picture was observed between crossed polarizers with a thin slice (about 100 μm thick) cut and polished carefully along the axis of the specimen. The axes of the polarizers are at $\pm 45°$ off the tensile direction. This micrograph shows a collection of small cavities at the centre of the necked region, whose black contrast is due to the refraction by the void surfaces inclined on the plane of the cut. This observation confirms the damage revealed by the density decrease at large strains. Furthermore, the two pairs of black fringes on each side of the neck should be noted. These extinction lines are due to the birefrigence of the oriented macromolecules. They are located where the optical paths for the two polarized components differ by a multiple of the mean wavelength (about 0.6 μm). Thus the two fringes, which correspond to the first and second order extinction, coincide with isodeformation lines. It is interesting to note that their curvature is weak. This indicates that, although a marked axial strain gradient is present in the shoulder of the neck, the radial strain gradient is quite moderate, especially in the middle of the neck. Consequently, the effective strain inhomogeneities in the median plane of the sample should be considered as small with respect to the current strain.

The hypothesis of constant volume, for its part, has been criticized from experimental results for polypropylene [34]: it has been shown that the total change of volume is less than 8% for a strain of 2.0 at 70 °C. Several interpretations have been proposed for this decrease of density. The first one holds for the elastic contribution to the total strain. It is well known that the elastic Poisson's ratio of polymers is of the order of 0.35, that is lower than the value required for incompressibility ($\nu = 0.5$). For the maximum stress recorded here and owing to the elastic modulus of polypropylene, the relative volume expansion corresponding to this effect can be shown to be less than 2.5%. More serious are the effects of the structural damage induced by the plastic deformation. It was shown previously (e.g. [34, 35]) that some crystallites may be fragmented while polypropylene is stretched, thus lowering the local density, in particular during the separation of the crystalline lamellae originally perpendicular to the tensile axis. This effect causes a typical whitening of the specimen often noticed in the literature. For example, in polybutene-1, it was shown from *in situ* experiments [36] that this whitening was actually initiated in the equatorial plane of the spherulites under tension. Also it is plausible that voids or crazes appear during deformation, due to the microscopic concentration of stress at the centre of the spherulites or at the interspherulitic boundaries. Whatever the origin of the density variations, it does affect the validity of the relation $\varepsilon = 2 \ln(D_0/D)$ which should be replaced, for a more rigorous analysis, by $\varepsilon = 2 \ln(D_0/D) + \Delta V/V$ [3]. Apart from the fact that $\Delta V/V$ is not available in real time in the present experiments, one can check that taking into account in the definition of ε, the actual volume variation, less than 8%, would merely affect the effective stress–strain curves by a very small reduction of the strain-hardening at large strains, that is decrease by less than 10% the parameter h.

For the treatment of stress, it should be emphasized that the main reason why the effective variable must be introduced (instead of the more simple Kirchoff stress) is because the samples undergoing a necking process adopt a curved profile, so that radial and circumferential stress components (σ_{rr} and $\sigma_{\theta\theta}$, respectively) develop locally. The rigorous prediction of the triaxial stress field in necked samples by finite-element numerical methods is not possible to date due to the complexity of the case of polymers: viscoelasticity, strain-rate sensitive plasticity, strain-hardening, deformation-induced damage, etc. Furthermore, this would require introduction into the computer code of the constitutive equation of the material, which is specifically what one wants to determine. Therefore, we will estimate the validity of the assumptions made in this work from semi-quantitative arguments drawn from simplified simulations performed previously. The first of them, a finite element approach, was developed by G'Sell *et al.* [11] for a material obeying an elasto-plastic constitutive equation and applied to the case of

high-density polyethylene. The simulation was capable of predicting the development of a neck up to large strains and of computing all the components of stress. The variations of the average axial and effective stress were thus derived in the plane of minimum cross-section, leading to the variations of the theoretical triaxiality factor. It was found that the computed F_T factor was of the correct order of magnitude, but systematically larger than the corresponding value deduced from the Bridgman formula. This discrepancy was attributed either to the limited number of finite elements in the mesh, or, more fundamentally to the neglect of the strain-rate sensitivity, which was not considered in the constitutive relation chosen to model the material. Conversely, the strain-rate sensitivity was taken into account by Laugier [13], who introduced the constitutive equation, in its multiplicative form, into a viscoplastic finite-element code (FORGE2®). Tensile testing of a polypropylene sample at a constant local strain rate was simulated, the triaxiality factor was computed as the function of strain and compared to the value given by the Bridgman equation. In such a case the computed factor was systematically lower than the Bridgman one.

Although the above studies are of conceptual interest and show that the finite element method is potentially able to solve the problems addressed here, its present state of development is not sufficient to draw precise conclusions about the errors introduced through the working assumptions. Nevertheless, all the simulations show that the correction brought to the Kirchoff stress by the Bridgman factor is correct in its sign ($F_T - 1 < 0$ for a concave curvature) and in its order of magnitude ($0.9 < F_T < 1$). Furthermore, it should be remarked that the largest deviations from Bridgman's assumptions (anisotropy, damage, hardening, etc.) are expected when the strain reaches very large values, that is when the specimen takes a quasi-homogeneous profile (Fig. 5) and the triaxiality factor approaches unity. We can then consider, like most authors in the current metallurgical literature, that the Bridgman factor is operationally acceptable in a first approximation for semi-crystalline polymers.

From the analysis developed above, several conclusions can be drawn.

(a) Although numerical simulations show that the effective strain suffers some variations in a given cross-section, the surfaces corresponding to constant values of ε are generally not too far from planar cross-sections [13]. Therefore Equation 8 is expected to give a correct estimate of the average effective strain in the minimum section.

(b) The constant volume assumption can be kept as a first approximation for a number of polymers. However, it would be useful to apply more sophisticated techniques in the testing system in order to measure in real-time the volume variation and to take into account this information in the measurement of ε.

(c) The choice of Bridgman's approach, for the estimation of the triaxiality effect, is not rigorously validated to date in the case of polymers. However, the use of a more elaborate formula would increase the complexity of the treatment without changing considerably the current value of σ.

(d) Consequently, the $\sigma(\varepsilon)$ curves determined in this work allow the determination of constitutive equations with a reasonable precision-to-complexity ratio. Such equations, which are macroscopic and phenomenological in nature, are likely to be used for the simulation of plastic instabilities during forming processes. As an example, we will examine later how the development of necks can be predicted during the stretching of axisymmetric test pieces. They can also help understanding the microscopic mechanisms and structural transformations which control the plastic behaviour of polymer, like the development of orientational textures along different deformation paths in semi-crystalline polymers [34, 35].

4.2. Validity of the constitutive equation

The choice of a multiplicative or an additive form for the constitutive equation is not really a problem, because both forms are nothing other than mathematical fits of the same set of experimental $\sigma(\varepsilon)$ curves obtained at different strain rates and temperatures. Both forms were actually utilized by Aly-Helal [5] in the case of high-density polyethylene. In the present work our choice of the multiplicative relation of Equation 14 results from its analogy with the Norton–Hoff law usually considered for metals

$$\sigma = K 3^{1/2} [3^{1/2} (\dot{\varepsilon}/\dot{\varepsilon}_0)]^m \quad (15)$$

where K holds for the "consistency" of the material. Identifying this expression with the one in Equation 14 leads to the following relation

$$K = k[1 - \exp(-w\varepsilon)] \exp(h\varepsilon^2) (3^{1/2})^{-m-1} \quad (16)$$

The major interest of this analogy is that it makes it possible to use viscoplastic computer codes, in which the solution of the mechanical problem consists in minimizing a functional of the velocity field. For instance, the code FORGE2® has been extensively used to model different problems of solid-state deformation

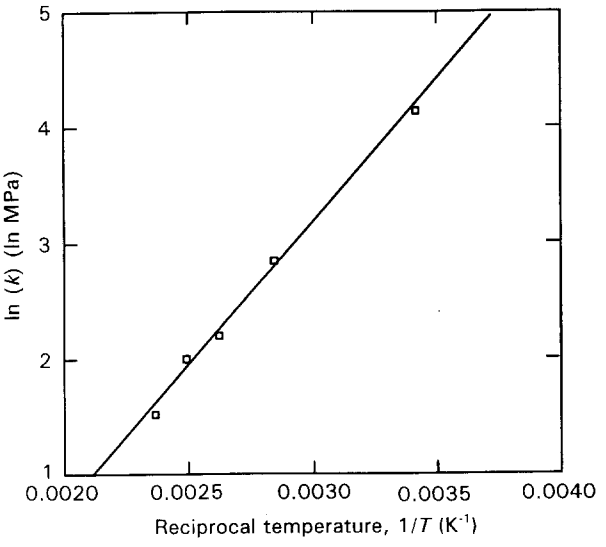

Figure 11 Variations of $\ln(k)$ as a function of $(1/T)$.

in metals and polymers [12–19]. In the case of anisothermal problems, it is assumed that the temperature dependence is essentially due to the scaling factor, k. This is a reasonable assumption, as it can be checked in Table II. Furthermore, the temperature dependence of k can be very conveniently modelled by an Arrhenius law, as shown in Fig. 11.

4.3. Application of the constitutive equation for the simulation of plastic instabilities

As a typical application of the constitutive equation, we will examine in this section the simulation of stretching instabilities in polypropylene at different temperatures by means of a finite-difference code developed by G'Sell *et al.* [1, 25]. Although this approach is restricted to the pseudo-uniaxial case of tension (by contrast to the sophisticated FEM codes which deal with fully triaxial cases) it is worthwhile to analyse it here because it can be run within a few minutes on the currently available microcomputers and predicts both the evolution of the specimen profile and the engineering stress–strain curves. It is thus an interesting tool to check the influence of specific parameters or in an extended version, to take into account the influence of adiabatic self-heating effects.

The one-dimensional geometry used in the model is illustrated in Fig. 12, the specimen being decomposed into N slices. Each individual element, normal to the axis, is assumed to deform homogeneously and to obey the constitutive equation introduced in Equation 14 with the set of parameters corresponding to the stretching temperature in Table II. The boundary conditions holding for the stretching process correspond to: (i) a constant overall elongation rate and, (ii) a zero strain rate for the material elements located at both extremities. The discretized form of the isothermal constitutive equation is then

$$\sigma_i = k[1 - \exp(-w\varepsilon_i)]\exp(h\varepsilon_i^2)(\dot{\varepsilon}_i/\dot{\varepsilon}_0)^m \quad (17)$$

where σ_i is the effective stress in the current slice labelled i. In the limit of slow stretching rates, the inertia effects can be neglected so that the mechanical equilibrium of the system is expressed through the constancy of the load along the sample according to the following expression

$$F = \sigma_{zz_i} A_i = \frac{\sigma_i A_i}{F_{T_i}} = \text{const} \quad (18)$$

where σ_{zz_i}, A_i and F_{T_i} are respectively the axial (Kirchoff) stress, the cross-sectional area and the triaxiality factor in the current slice.

In the finite-difference scheme used, the total elongation rate $\dot{L} = dL/dt$ of the sample, which is held constant during the simulation, is given by

$$\frac{\dot{L}}{L_0} = \sum_{i=1}^{N} \frac{\dot{L}_i}{L_0} = \sum_{i=1}^{N} \frac{L_{0i}}{L_0}\exp(\varepsilon_i)\dot{\varepsilon}_i \quad (19)$$

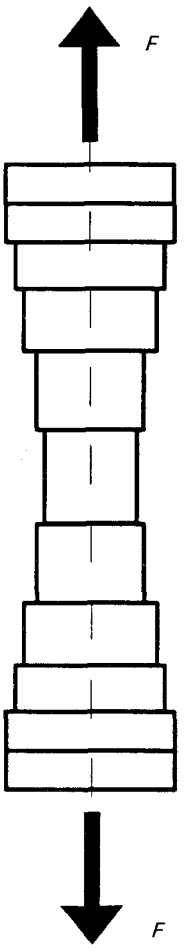

Figure 12 Finite-difference discretization of the tensile specimen.

where $\dot{L}_i$, L_{0i} are the elongation rate and initial length, ε_i, $\dot{\varepsilon}_i$ are the strain and strain rate of each slice, and L_0 is the initial length of the sample. Combining Equations 17, 18 and 19 gives the strain rate in each element

$$\dot{\varepsilon}_i = \frac{\dot{L}}{L_0}\left\{\sum_{j=1}^{N}\frac{L_{0j}}{L_0}\exp(\varepsilon_j)\left[\frac{A_i}{A_j}\frac{1-\exp(-w\varepsilon_i)}{1-\exp(-w\varepsilon_j)}\frac{\exp(h\varepsilon_i^2)}{\exp(h\varepsilon_j^2)}\frac{F_{T_j}}{F_{T_i}}\right]^{1/m}\right\}^{-1} \quad (20)$$

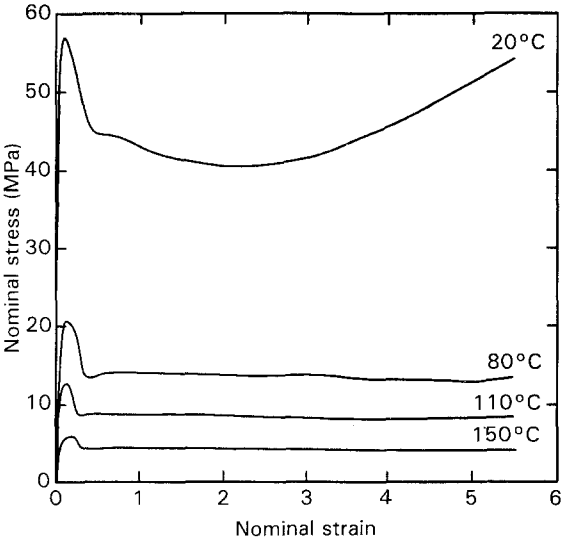

Figure 13 Simulated engineering stress–strain curves at different temperatures.

The value of the strain rate, $\dot{\varepsilon}_i$, is calculated directly and integrated over the time step, δt, corresponding to a given increment of the length, δL. These steps are adjusted dynamically in the course of the computation in such a way that the maximum strain increment $\delta\varepsilon_i$ is equal to 0.03. The number of elements, N, is chosen equal to 120. The rheological coefficients introduced in the code (k, w, h, and m) are those determined experimentally for the polypropylene at the prescribed temperature, as displayed in Table II.

The engineering stress–strain curves ($\sigma_e = F/A_0$ versus $\varepsilon_e = (L - L_0)/L_0$), obtained with the simulation code at different temperatures, are displayed in Fig. 13. Also the simulated kinetics of necking during

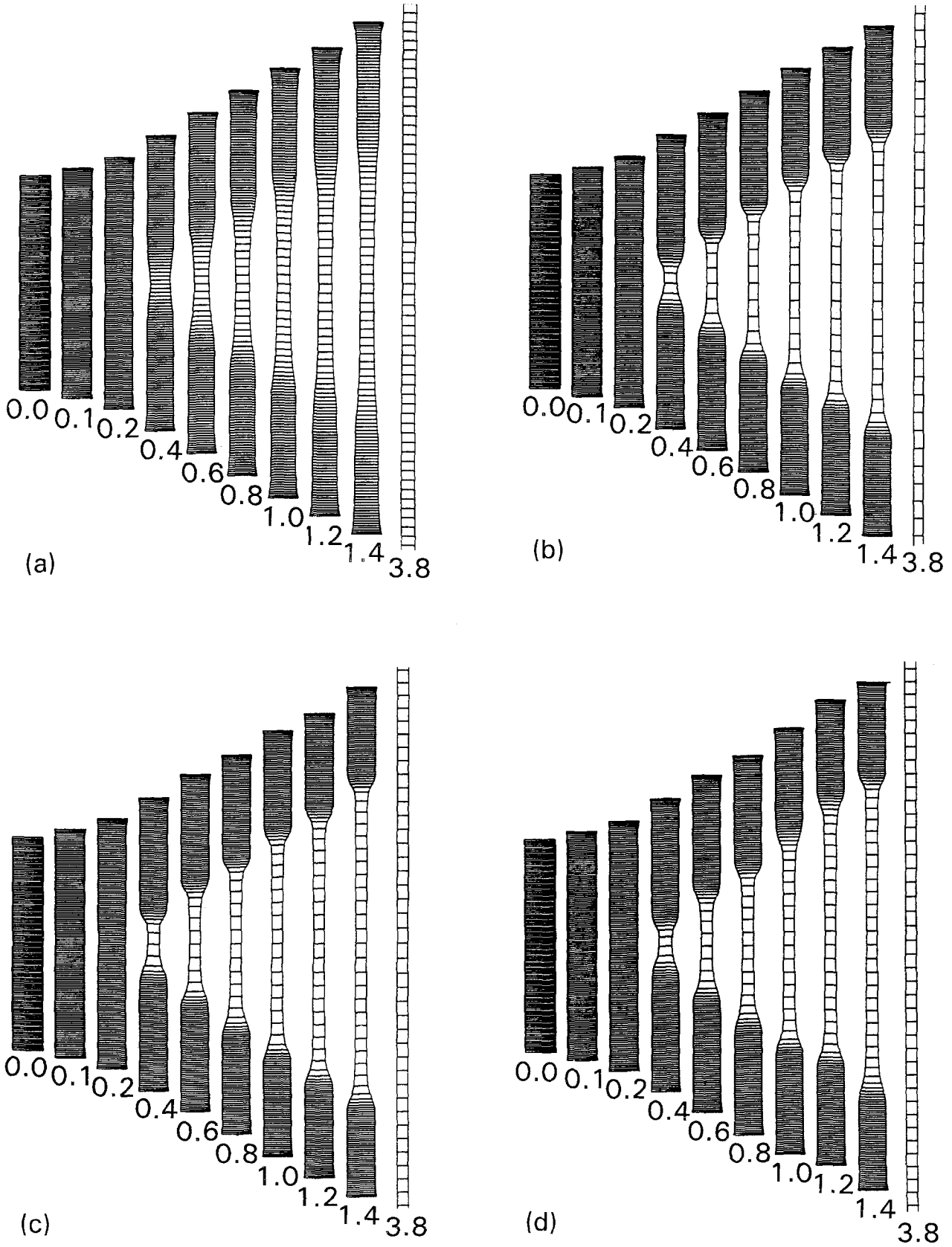

Figure 14 Simulated kinetics of necking, during the drawing, obtained from the model at different temperatures (numbers indicate the nominal strain). (a) $T = 20\,°C$, (b) $T = 80\,°C$, (c) $T = 110\,°C$, (d) $T = 150\,°C$.

the stretching of the polypropylene is represented in Fig. 14. One notes that all the features of the experimental behaviour are reproduced by the simulation including the load maximum at the yield point, the sharp strain softening which occurs while the neck is formed, the stress plateau corresponding to the neck propagation and the final hardening at large strains. It is interesting to note that plastic instabilities occur at all the temperatures investigated, even at the approach of the melting point (see, for example, the sharp profiles at 150 °C even though the effective stress–strain curve displays a very progressive yielding). This is because, even at elevated temperature, the Considère criterion (corresponding to the critical condition $d\sigma/d\varepsilon < \sigma$) is verified early at the central cross-section of the sample and that the stabilization ($d\sigma/d\varepsilon > \sigma$) occurs lately when the effective stress–strain curve eventually shows a significant strain hardening. Unexpectedly, it is even observed that the development of the neck is more important at elevated temperatures than at 20 °C. This is because the ultimate strain-hardening occurs much earlier at room temperature than at elevated temperature and that the strain-rate sensitivity, m, is globally lower when the temperature is higher. This destabilizing effect of temperature is not a general property of polymers. In the case of amorphous thermoplastics, for example, it is known that plastic instabilities progressively disappear when approaching T_g because the yield point decreases faster than the large strain-hardening and the strain-rate sensitivity coefficient increases.

References

1. C. G'SELL, *Rev. Phys. Appl.* **23** (1988) 1085.
2. G. MEINEL and A. PETERLIN, *J. Polymer Sci. A2* **9** (1971) 67.
3. C. G'SELL and J. J. JONAS, *J. Mater. Sci.* **14** (1979) 583.
4. *Idem, ibid.* **16** (1981) 1956.
5. N. A. ALY-HELAL, Thesis, Institut National Polytechnique de Lorraine, Nancy (1982).
6. C. G'SELL, N. A. ALY-HELAL and J. J. JONAS, *J. Mater. Sci.* **18** (1983) 1731.
7. D. COTTO, F. MONTHEILLET and J. M. HAUDIN, *Compt. Rend. Acad. Sci. Paris* **298** (II) (1984) 511.
8. *Idem, ibid.* **301** (II) (1985) 885.
9. *Idem*, in "Proceedings of the International Symposium on Plastic Instability", Considère Memorial, Presses des Ponts et Chaussées (Paris, 1985) p. 79.
10. K. W. NEALE and P. TUGCU, *J. Mech. Phys. Solids* **33** (1985) 323.
11. C. G'SELL, A. MARQUEZ-LUCERO, A. SOUAHI and Y. S. TONG, in "Proceedings of the International Symposium on Plastic Instability", Considère Memorial, Presses des Ponts et Chaussées, (Paris, 1985) p. 159.
12. M. LAUGIER, T. VALLA, E. WEY, J. M. HAUDIN and J. L. CHENOT, in "Proceedings of the Second International Conference on Advances in Numerical Methods in Engineering: Theory and Applications", NUMETA '87 (Swansea, 1987), edited by G. N. Pande and J. Middleton (Martinus Nijhoff, Dordrecht, 1987) p. C1/1.
13. M. LAUGIER, Thesis, Conservatoire National des Arts et Métiers, Aix-en-Provence (1988).
14. P. DUFFO, B. MONASSE, J. L. CHENOT and J. M. HAUDIN, in "Proceedings of the Third International Conference on Advances in Numerical Methods in Engineering: Theory and Applications", Vol. 2, NUMETA '90 (Swansea, 1990), edited by G. N. Pande and J. Middleton (Elsevier Applied Science, London, 1990) p. 769.
16. B. MONASSE, M. LAUGIER, J.-M. HAUDIN and J. L. CHENOT, in "Proceedings of the Fifth Annual Meeting of the Polymer Processing Society" (Kyoto, 1989) p. 170.
17. B. MONASSE, J. M. HAUDIN and J. L. CHENOT, in "Proceedings of the Third International Conference on Technology of Plasticity", Vol. 1 (Kyoto, 1990) p. 247.
18. T. VALLA, B. MONASSE, J. M. HAUDIN and S. GLOMMEAU, in "Proceedings of the Sixth Annual Meeting of the Polymer Processing Society" (Nice, 1990) paper 11-01.
19. N. BILLON and J. M. HAUDIN, in "Proceedings of the International Conference on Numerical Methods in Industrial Forming Processes", NUMIFORM '92 (Sophia-Antipolis, 1992), edited by J. L. Chenot, R. D. Wood and O. C. Zienkiewicz (A. A. Balkema, Rotterdam, 1992) p. 335.
20. B. WUNDERLICH, "Macromolecular Physics", Vol. 3, "Crystal Melting" (Academic Press, New York, 1980) p. 48.
21. E.SIEBEL, *Werkstoff.* **71** (1925) 5.
22. P. W. BRIDGMAN, *Trans. Am. Soc. Met.* **32** (1944) 553.
23. N. N. DAVIDENKOV and N. I. SPIRIDONOVA, *Proc. Am. Soc. Test. Mater.* **46** (1946) 1147.
24. N. J. MILLS, *Br. Polym. J.* **10** (1978) 1.
25. C. G'SELL, N. A. ALY-HELAL, S. L. SEMIATIN and J. J. JONAS, *Polymer* **33** (1992) 1244.
26. C. G'SELL, J. M. HIVER, A. DAHOUN and A. SOUAHI, *J. Mater. Sci.* **27** (1992) 5031.
27. A. MARQUEZ-LUCERO, C. G'SELL and K.W. NEALE, *Polymer* **30** (1989) 636.
28. A. K. GHOSH, *Metall. Trans.* **8A** (1977) 1221.
29. *Idem, Acta Metall.* **25** (1977) 1413.
30. J. M. ANDREWS and I. M. WARD, *J. Mater. Sci.* **5** (1970) 411.
31. I. M. WARD, *ibid.* **6** (1971) 1397.
32. J. M. HAUDIN, in "Plastic Deformation of Amorphous and Semi-Crystalline Materials", edited by B. Escaig and C. G'Sell (Les Editions de Physique, les Ulis, France, 1982) p. 291.
33. A. S. ARGON, J. IM and A. NEEDLEMAN, *Metall. Trans.* **6A** (1975) 815.
34. A. DAHOUN, Thesis, Institut National Polytechnique de Lorraine, Nancy (1992).
35. C. G'SELL and A. DAHOUN, *Mater. Sci. Eng*, **A175** (1994) 183.
36. E. WEYNANT, J. M. HAUDIN and C. G'SELL, *J. Mater. Sci.* **15** (1980) 2677.

Received 31 January
and accepted 9 June 1994